Structural Control & Health Monitoring
The Journal of the International Association for Structural Control and Monitoring

Structural system identification by Measurement Error-Minimizing Observability Method

Journal:	*Structural Control and Health Monitoring*
Manuscript ID	STC-18-0102.R2
Wiley - Manuscript type:	Research Article
Date Submitted by the Author:	12-Jun-2019
Complete List of Authors:	Lei, Jun; Tongji University, Department of Bridge Engineering Lozano Galant, Jose Antonio; University of Castilla-La Mancha, Department of Civil Engineering Xu, Dong; Tongji University, Department of Bridge Engineering Turmo, Jóse; Universitat Politecnica de Catalunya, Department of Civil and Environmental Engineering
Keywords:	Static, Observability Method, Fisher Information Method, Optimization, Null Curvature, Rotations

Structural System Identification by Measurement Error-Minimizing Observability Method

Given Name	Surname	Institutions
Jun	LEI	Department of Bridge Engineering, Tongji University, Shanghai 200092, China
Jose Antonio	Lozano-Galant	Department of Civil Engineering, University of Castilla -La Mancha, Ciudad Real 13071, Spain
Dong	XU	Department of Bridge Engineering, Tongji University, Shanghai 200092, China
Jose	Turmo	Department of Civil and Environmental Engineering, Universitat Politècnica de Catalunya, Barcelona 08034, Spain

Corresponding author: Dong XU

Address: Department of Bridge Engineering, Tongji University, 1239 Siping Road, 200092, Shanghai, China

Email: xu_dong@tongji.edu.cn

Tel.: +86 21 65983116 ext.2506;

Fax: +86 21 65986507.

Structural System Identification by Measurement Error-Minimizing Observability Method

Jun LEI, Jose Antonio Lozano-Galant, Dong XU, Jose Turmo

Abstract:

This paper proposes a method for the finite element model updating using static load tests under the framework of observability analysis. Previous works included measurement errors in the coefficient matrix of the observability equations. This impeded the obtainment of accurate estimations. To deal with this issue, the proposed method relocates the errors and incorporates an optimization procedure to minimize the square sum of these errors. This method is able to identify the structural parameters of complex structures where the axial and the bending behaviors are coupled, such as inclined beams or frame structures. Its application is illustrated by three structures. First, the method was validated in a beam-like structure by comparing it with other methods in the literature. Then the effects of different factors were investigated in a multi-story frame and a rigid frame bridge with inclined piers. These factors include the curvatures, the inclusion of rotation measurements and the constraints on the range of unidentifiable parameters. The importance of rotation measurements is demonstrated in static SSI.

1 Introduction

Structural health monitoring has become a powerful tool to help decision making during life cycle of civil and infrastructure systems[1]. As a key component of structural health monitoring, Structural System Identification (SSI) aims to identify the parameters of a mathematical model that links the measured response and the external excitation of a structure. It is commonly assumed that the degradation of structures is reflected in the change of these parameters[2].

According to the intrinsic characteristics of the structural response, SSI can be classified as static SSI[3–14] or dynamic SSI[15–20]. Compared with static SSI, dynamic SSI has been developed more extensively in the past decades. Depending on the source of excitation, dynamic methods can be classified as input-output[19] and output-only[15,17,18] methods. In the output-only methods, the response due to operational load (wind or traffic) is measured and interruption of traffic or normal operation is not necessary. On the contrary, the static methods or the input-output dynamic methods require the excitation information, such as the magnitude and location of the static forces or shakers. Different dynamic SSI methods have been proposed and studied for the purpose of damage detection and quantification. Numerous algorithms using different indices have been developed, such as natural frequencies[16], mode shapes[17], modal curvature[20], and high-order mode shape derivative[19].

Despite the wide application of dynamic SSI methods, this research is going to focus on static SSI for the following reasons: (1) the physical equations involved with static SSI are only related to the structural stiffnesses while those involved with dynamic SSI are also related to the mass and the damping of the structure[21]. The damping information is commonly obtained by analyzing the vibration test data. Meanwhile, the mass information is estimated from the drawings. The difficulties involved with obtaining accurate damping and mass information may well introduce more uncertainties and modelling errors in the dynamic based structural health monitoring. (2) The solution for measuring static displacements is easier, cheaper and have higher accuracy than those for dynamic

SSI[22]. (3) Dynamic characteristics (e.g. frequencies) are insensitive to local structure damages due to the fact that they mainly reflect the global and distributed phenomenon of the structure[23]. Static methods might have higher sensitivity to local damages.

Static SSI methods have attracted notable consideration recently. Sheena obtained the stiffness matrix using measured displacements and minimized the deviation between the estimated stiffness matrix and the analytical one[5]. Sanayei and Onipede presented an iterative optimization-based algorithm to displacement equation error function for the parameter estimations using static measurements. Bakhtiari-Nejad presented a method to describe changes in static displacements with certain degrees of freedom by minimizing the difference between the load vectors of damaged and undamaged structures[3]. Banan proposed an optimization method to estimate member constitutive properties of the Finite Element Model (FEM), from measured displacements under static loading[6]. Sanayei updated the FEM of a 47-m bridge using 100 strain gauges with static truck loads[10]. A new direction in static SSI method arises from using static or quasi-static displacement influence lines. Choi used the elastic damage load theorem for statically determinate beam to locate the damage by checking the deflection variations[11]. This method is limited to statically determinate structures and cannot quantify the extent of the damage. Abdo combined the grey relation coefficient and the changes in static deflections curvature to locate the damage[12]. Using the influence line principle with a static moving load, Nadir approximated the stiffness matrix with Neumann series[13]. This method is able to locate the damage and evaluate the damage extent when the noise level is low. Sun used curvature changes from the static component of displacement measurements under a moving vehicle to detect damage in bridges during field test[14]. However, these methods mainly use the sudden change of the influence lines to locate the damages and the relevant quantification of damage extent is lacking. Also, it should be pointed out that in the majority of static SSI, the adopted measurements mainly contain strains or deflections while rotations are rarely measured. However, wide applications of inclinometers can be found in civil engineering practice, such as stadiums *Design Plaza Building*[24], high-rise buildings[25], and bridges[26,27]. In the study of the effect of measurement types on the estimation accuracy in a 4-node simply-supported beam, it was found that the rotations were much less sensitive to errors than the vertical deflections[28]. However, systematic investigation on the effect of including rotation measurements on the estimation accuracy in static SSI is lacking.

In the SSI or state estimation literature, observability is a measure for how well internal states of a system can be inferred by knowledge of its external outputs. In the case of dynamic SSI using state-space form, this can be done by checking the rank of the observability matrix[29]. Lately, the technique to address observability in static SSI under controlled loads was proposed by Lozano[4]. Regarding a given measurement set, the stiffness matrix method and the observability method (OM) with the null space approach[30] were combined to determine the existence and uniqueness of the structural parameters symbolically. The method was applied to identify plane beam element models loaded in its plane[4]. The observability of the structural system depends on the number and the location of measurements. Specially, measurement sets are defined as *essential sets*[7] when: (1) they have exactly as many measurements as the number of structural parameters to be estimated; (2) they are able to identify all target parameters and the drop of any measurement fails to do so. These essential sets can be found via SSI by Constrained OM[7]. In previous study, the estimation accuracy using essential sets are not satisfactory when measurement error exists[28]. Hence, *redundant sets* (essential sets plus redundant measurements) are used to reduce estimation errors. In beam-like structures, the compatibility conditions (the geometrical relations that the displacements should satisfy) can be obtained symbolically via SSI by compatible OM[31]. These conditions can be used to improve estimation accuracy. However, the current formulation of SSI by OM cannot be applied in structures

where bending behaviors and axial behaviors are coupled. This limits the application of the method in frame structures.

In this paper, a different formulation of the observability equations is proposed to deal with measurement errors in the static SSI of structures where the axial and the bending behaviors are coupled. In the new formulation, the measurement errors are separated from the coefficient matrix and moved to the unknowns, forming a new system of observability equations. Then the square sum of all error terms is minimized by an optimization procedure while nonlinear relations among the unknowns are imposed. To fill the gap in the study on measurement types, this paper will also investigate the effect of including rotation measurements in static SSI using the proposed method. The effects of the parameterization of FEM, the curvature and the bounds imposed on the parameters are also analyzed and discussed.

In the remainder of this paper, section 2 briefly introduces the static SSI by constrained OM. Then the procedure for the proposed measurement error-minimizing observability method (MEMOM) is illustrated by an academic example. The sensor placement is determined by the Fisher Information matrix together with a genetic algorithm. In section 3, the performance of the proposed method is validated in a beam-like structure. The estimations obtained from *essential sets* and *redundant sets* are compared with those obtained by the numerical OM[32] and the compatible OM[31], respectively. In addition, a table summarizing the characteristics of these methods is provided at the end of this section. In section 4, the effectiveness of the proposed method is verified in a large frame and a rigid frame bridge. The last section summarizes the key findings and concludes the paper.

2 Methodology

2.1 Structural system identification by constrained observability method

Static SSI by Constrained OM imposes constraints on variables when no more parameters can be observed using SSI by OM. The identical part between these two methods is introduced first and their difference is pointed out at the end of this section.

In static SSI by OM, a FEM has to be defined first. The equilibrium equations Eq. (1) are then established. For 2D beam element models, due to the equilibrium of forces on each node in horizontal, vertical and rotational directions, the number of equations N_{eq} is three times the number of nodes N_n, i.e. $N_{eq}=3N_n$,.

$$[K] \cdot \{\delta\} = \{f\} \tag{1}$$

In this system, the global stiffness matrix $[K]$ includes both the geometrical and the mechanical properties of element j (i.e. length L_j, elastic moduli E_j, area A_j and inertia I_j, j=1, 2, …, N_e; where N_e is the number of elements). The displacement vector $\{\delta\}$ includes horizontal displacements u_i, vertical deflections v_i, rotations w_i of node i (i=1, 2, …, N_n; where N_n is the number of nodes). The right-hand side vector $\{f\}$ includes horizontal forces H_i, vertical forces V_i, and moments M_i on node i. Hence, all the variables appearing in the equations are (E_j, A_j, I_j, L_j, u_i, v_i, w_i, H_i, V_i and M_i). The objective of SSI is to identify structural parameters θ (such as axial stiffness E_jA_j or bending stiffness E_jI_j) so as to assess the condition of the structure by the values of θ. To reduce unknowns, these stiffnesses, E_jA_j and E_jI_j are treated as linearized unknowns, EA_j and EI_j, and L_j is usually assumed as known. In addition, during the static test, the controlled static loads are known and some resulting increments of the displacements $\tilde{\delta}$ have to be measured.

These parameters appear in matrix $[K]$ as monomial ratios, such as $\frac{EA_j}{L_j}$, $\frac{EI_j}{L_j^2}$ or $\frac{EI_j}{L_j^3}$. As some elements of vector $\{f\}$ are also unknowns, nonlinearity arises in the system of equations. Hence, the system is linearized by a series of algebraic operations[4], as shown in Eq. (2).

$$[K^*]\cdot\{\delta^*\}=\begin{bmatrix}K_{10}^* & K_{11}^*\\ K_{00}^* & K_{01}^*\end{bmatrix}\begin{Bmatrix}\delta_0^*\\ \delta_1^*\end{Bmatrix}=\begin{Bmatrix}f_1\\ f_0\end{Bmatrix}=\{f\} \tag{2}$$

The remaining coefficient matrix $[K^*]$ are composed of constants that are either zero or the powers of the inverse of L_j. Once the loads and the measurements from the static test as well as the boundary conditions of the structure have been defined, it is assumed that a subset $\{\delta_1^*\}$ of $\{\delta^*\}$ and a subset $\{f_1\}$ of $\{f\}$ are known while remaining subset $\{\delta_0^*\}$ of $\{\delta^*\}$ and $\{f_0\}$ of $\{f\}$ are not. To cluster the unknowns together, Eq. (2) is transformed to Eq. (3) by static condensation.

$$[B]\cdot\{z\}=\begin{bmatrix}K_{10}^* & 0\\ K_{00}^* & -I\end{bmatrix}\begin{Bmatrix}\delta_0^*\\ f_0\end{Bmatrix}=\begin{Bmatrix}f_1-K_{11}^*\delta_1^*\\ -K_{01}^*\delta_1^*\end{Bmatrix}=\{D\} \tag{3}$$

In Eq. (3), both the coefficient matrix $[B]$ and the right-hand side vector $\{D\}$ are completely known. The coefficient matrix $[B]$ is composed of either zero or monomial ratios of knowns (measured displacements, known stiffnesses and element lengths). Meanwhile, the right-hand side vector $\{D\}$ is composed of the external loads $\{f_1\}$ and the equivalent nodal forces ($K_{11}^*\delta_1^*$ or $K_{01}^*\delta_1^*$). On the other hand, the unknowns $\{z\}$ are of two types: (1) node displacements, (u_i, v_i or w_i), or parameters θ, (EA_j or EI_j), or the products of both, (EA_ju_i, EA_jv_i, EA_jw_i, EI_ju_i, EI_jv_i or EI_jw_i); (2) unknown reactions, (H_i, V_i and M_i), at the boundary conditions. When Eq. (3) has at least one solution, the solution is the sum of a particular solution $\{z_p\}$, and the product of a vector of arbitrary values, $\{\rho\}$, and the null space $[N]$ of the coefficient matrix $[B]$ in Eq. (3).

$$\{z_g\}=\{z_p\}+[N]\cdot\{\rho\}=\begin{Bmatrix}\delta_0^*\\ f_0\end{Bmatrix}_p+[N]\cdot\{\rho\} \tag{4}$$

The particular solution $\{z_p\}$ is the pseudo inverse solution of Eq. (3). $[N]\cdot\{\rho\}$ is the set of all solutions of the associated homogeneous system of equations (a linear space of solutions, wherein the columns of N are vectorial bases, and the entries of the vector $\{\rho\}$ are arbitrary values functioning as the coefficients of all possible linear combinations). If any row of the null space $[N]$ is composed of only zeros, then the scalar in the same row of the product $[N]\cdot\{\rho\}$will be zero, and thereby the particular solution specifies the unique solution for that parameter. Namely, any unknown associated with a zero row in the null space $[N]$ is observable, i.e. it exists and it is determined and unique. All these observable unknowns are introduced as known in the next step to obtain updated observability equations and thus new parameters might be observed. To obtain the values of these observable parameters, it is necessary to append the numerical approach proposed by Nogal[32].

It should be pointed out that all unknowns are treated as linear when applying the algebraic operations. This is essential for observability analysis. However, it leads to the loss of information because the equality between coupled unknowns and the product of the associated components, for instance, $EI_2w_2=EI_2\cdot w_2$, is missing due to the linearization of the variable EI_2w_2. To deal with this issue, SSI by Constrained OM imposes these lacking constraints by an optimization procedure. In the numerical optimization, the objective function is to minimize the square sum of the residuals (equilibrium forces) of the observability equations from the last recursive step in SSI by OM while forcing the equality

between the coupled variable and the product of its components[7]. This method is used to find the essential sets in static SSI[7,8].

2.2 Formulation of the system of observability equations by separating the errors

The coefficient matrix of the observability equations (Eq. (3)) takes in the measurements together with the errors, which is a perturbation to the accurate matrix. Previous study shows that the least square solution of observability equations is greatly biased even with redundant sets[31]. This section proposes a measurement error-minimizing observability method (MEMOM). For the very first time, measurement errors are separated from the coefficient matrix and then included in the unknown vector so as to eliminate the adverse effect of errors in the coefficient matrix.

For illustrative purpose, the necessary procedures to implement the proposed method are demonstrated below by an academic example. Consider a 10-m simply supported beam. Its FEM has two elements of length L=5m. The boundary conditions are that u_1=v_1=v_3=0. The FEM is parameterized by two bending stiffnesses, EI_1 and EI_2, and two axial stiffnesses, EA_1 and EA_2, as depicted in Fig. 1.

Without loss of generality, it is assumed that a vertical load V_2 is applied at midspan (Node 2) and the increments of displacements (w_1, v_2, and w_3) are measured. The necessary steps to implement the MEMOM are presented below.

Step 1. **Introduce the geometry, as well as the known mechanical and geometrical properties and external forces to establish an FEM for the structure. Build the equilibrium equations for this FEM.**

The equilibrium equations for this FEM are given in Eq. (5).

$$\begin{pmatrix} \frac{EA_1}{L} & 0 & 0 & -\frac{EA_1}{L} & 0 & 0 & 0 & 0 & 0 \\ 0 & \frac{12EI_1}{L^3} & \frac{6EI_1}{L^2} & 0 & -\frac{12EI_1}{L^3} & \frac{6EI_1}{L^2} & 0 & 0 & 0 \\ 0 & \frac{6EI_1}{L^2} & \frac{4EI_1}{L} & 0 & -\frac{6EI_1}{L^2} & \frac{2EI_1}{L} & 0 & 0 & 0 \\ -\frac{EA_1}{L} & 0 & 0 & \frac{EA_1+EA_2}{L} & 0 & 0 & -\frac{EA_2}{L} & 0 & 0 \\ 0 & -\frac{12EI_1}{L^3} & -\frac{6EI_1}{L^2} & 0 & \frac{12EI_1}{L^3}+\frac{12EI_2}{L^3} & \frac{6EI_2}{L^2}-\frac{6EI_1}{L^2} & 0 & -\frac{12EI_2}{L^3} & \frac{6EI_2}{L^2} \\ 0 & \frac{6EI_1}{L^2} & \frac{2EI_1}{L} & 0 & \frac{6EI_2}{L^2}-\frac{6EI_1}{L^2} & \frac{4EI_1}{L}+\frac{4EI_2}{L} & 0 & -\frac{6EI_2}{L^2} & \frac{2EI_2}{L} \\ 0 & 0 & 0 & -\frac{EA_2}{L} & 0 & 0 & \frac{EA_2}{L} & 0 & 0 \\ 0 & 0 & 0 & 0 & -\frac{12EI_2}{L^3} & -\frac{6EI_2}{L^2} & 0 & \frac{12EI_2}{L^3} & -\frac{6EI_2}{L^2} \\ 0 & 0 & 0 & 0 & \frac{6EI_2}{L^2} & \frac{2EI_2}{L} & 0 & -\frac{6EI_2}{L^2} & \frac{4EI_2}{L} \end{pmatrix} \begin{pmatrix} u_1 \\ v_1 \\ w_1 \\ u_2 \\ v_2 \\ w_2 \\ u_3 \\ v_3 \\ w_3 \end{pmatrix} = \begin{pmatrix} H_1 \\ V_1 \\ M_1 \\ H_2 \\ V_2 \\ M_2 \\ H_3 \\ V_3 \\ M_3 \end{pmatrix} \tag{5}$$

Step 2: **Obtain the observability equations $[\boldsymbol{B}] \cdot \{\boldsymbol{z}\} = \{\boldsymbol{D}\}$.**

Introduce the boundary conditions into Eq. (5) and rearrange the equations such that all the unknowns are collected in the new unknown vector $\{z\}$, and both the coefficient matrix $[B]$ and right-hand side vector $\{D\}$ are known, as shown in Eq. (3).

Without loss of generality, the observability equations related with the measurement set (w_1, v_2 and w_3) are obtained from Eq. (5) by a series of algebraic operations. In this system of equations, the measurements are absorbed in the coefficient matrix. Provided that error-free measurements are used, this system of equations holds stringently. Denote the error-free displacements by a hat, ^. This relation is demonstrated by Eq. (6).

$$\begin{pmatrix} 0 & 0 & -\frac{6\hat{v}_2}{L^2} & \frac{4\hat{w}_1}{L} & \frac{2}{L} & 0 & 0 & 0 & 0 & 0 & 0 \\ \frac{2}{L} & -\frac{1}{L} & 0 & 0 & 0 & 0 & 0 & 0 & 0 & 0 & 0 \\ 0 & 0 & \frac{12\hat{v}_2}{L^3} & -\frac{6\hat{w}_1}{L^2} & -\frac{6}{L^2} & \frac{12\hat{v}_2}{L^3} & \frac{6}{L^2} & \frac{6\hat{w}_3}{L^2} & 0 & 0 & 0 \\ 0 & 0 & -\frac{6\hat{v}_2}{L^2} & \frac{2\hat{w}_1}{L} & \frac{4}{L} & \frac{6\hat{v}_2}{L^2} & \frac{4}{L} & \frac{2\hat{w}_3}{L} & 0 & 0 & 0 \\ -\frac{1}{L} & \frac{1}{L} & 0 & 0 & 0 & 0 & 0 & 0 & 0 & 0 & 0 \\ 0 & 0 & 0 & 0 & 0 & \frac{6\hat{v}_2}{L^2} & \frac{2}{L} & \frac{4\hat{w}_3}{L} & 0 & 0 & 0 \\ -\frac{1}{L} & 0 & 0 & 0 & 0 & 0 & 0 & 0 & -1 & 0 & 0 \\ 0 & 0 & -\frac{12\hat{v}_2}{L^3} & \frac{6\hat{w}_1}{L^2} & \frac{6}{L^2} & 0 & 0 & 0 & 0 & -1 & 0 \\ 0 & 0 & 0 & 0 & 0 & -\frac{12\hat{v}_2}{L^3} & -\frac{6}{L^2} & -\frac{6\hat{w}_3}{L^2} & 0 & 0 & -1 \end{pmatrix} \begin{pmatrix} EA_1u_2 \\ EA_2u_3 \\ EI_1 \\ EI_1 \\ EI_1w_2 \\ EI_2 \\ EI_2w_2 \\ EI_2 \\ H_1 \\ V_1 \\ V_3 \end{pmatrix} = \begin{pmatrix} M_1 \\ H_2 \\ V_2 \\ M_2 \\ H_3 \\ M_3 \\ 0 \\ 0 \\ 0 \end{pmatrix} \tag{6}$$

Step 3: **Include the error terms in the coefficient matrix [*B*].**

In real life, the measurements are always contaminated by errors. These measurements $\tilde{\delta}$ comprise of the error-free displacements $\hat{\delta}$ and the errors ϵ_δ. This relation can be rearranged as Eq. (7).

$$\hat{\delta} = \tilde{\delta} - \epsilon_\delta \tag{7}$$

Replace the error-free displacements $\hat{\delta}$ in the coefficient matrix $[B]$ of Eq. (6) by the difference of the measured displacements $\tilde{\delta}$ and the measurement errors ϵ_δ, Eq. (7). The resulting system of equations is given in Eq. (8)

$$\begin{pmatrix} 0 & 0 & -\frac{6(\tilde{v}_2-\epsilon_{v2})}{L^2} & \frac{4(\tilde{w}_1-\epsilon_{w1})}{L} & \frac{2}{L} & 0 & 0 & 0 & 0 & 0 & 0 \\ \frac{2}{L} & -\frac{1}{L} & 0 & 0 & 0 & 0 & 0 & 0 & 0 & 0 & 0 \\ 0 & 0 & \frac{12(\tilde{v}_2-\epsilon_{v2})}{L^3} & -\frac{6(\tilde{w}_1-\epsilon_{w1})}{L^2} & -\frac{6}{L^2} & \frac{12(\tilde{v}_2-\epsilon_{v2})}{L^3} & \frac{6}{L^2} & \frac{6(\tilde{w}_3-\epsilon_{w3})}{L^2} & 0 & 0 & 0 \\ 0 & 0 & -\frac{6(\tilde{v}_2-\epsilon_{v2})}{L^2} & \frac{2(\tilde{w}_1-\epsilon_{w1})}{L} & \frac{4}{L} & \frac{6(\tilde{v}_2-\epsilon_{v2})}{L^2} & \frac{4}{L} & \frac{2(\tilde{w}_3-\epsilon_{w3})}{L} & 0 & 0 & 0 \\ -\frac{1}{L} & \frac{1}{L} & 0 & 0 & 0 & 0 & 0 & 0 & 0 & 0 & 0 \\ 0 & 0 & 0 & 0 & 0 & \frac{6(\tilde{v}_2-\epsilon_{v2})}{L^2} & \frac{2}{L} & \frac{4(\tilde{w}_3-\epsilon_{w3})}{L} & 0 & 0 & 0 \\ -\frac{1}{L} & 0 & 0 & 0 & 0 & 0 & 0 & 0 & -1 & 0 & 0 \\ 0 & 0 & -\frac{12(\tilde{v}_2-\epsilon_{v2})}{L^3} & \frac{6(\tilde{w}_1-\epsilon_{w1})}{L^2} & \frac{6}{L^2} & 0 & 0 & 0 & 0 & -1 & 0 \\ 0 & 0 & 0 & 0 & 0 & -\frac{12(\tilde{v}_2-\epsilon_{v2})}{L^3} & -\frac{6}{L^2} & -\frac{6(\tilde{w}_3-\epsilon_{w3})}{L^2} & 0 & 0 & -1 \end{pmatrix} \begin{pmatrix} EA_1u_2 \\ EA_2u_3 \\ EI_1 \\ EI_1 \\ EI_1w_2 \\ EI_2 \\ EI_2w_2 \\ EI_2 \\ H_1 \\ V_1 \\ V_3 \end{pmatrix} = \begin{pmatrix} M_1 \\ H_2 \\ V_2 \\ M_2 \\ H_3 \\ M_3 \\ 0 \\ 0 \\ 0 \end{pmatrix} \tag{8}$$

Step 4: **Obtain the new system of equations including error terms, $\boldsymbol{B_e \cdot z_e = D}$** (Eq. (9)).

This step is similar to the algebraic techniques used for the linearization of the observability equations. Each column containing $\tilde{\delta} - \epsilon_\delta$ is separated into two columns, where one is related to the error-free displacement $\tilde{\delta}$ and the other is related to the error term ϵ_δ. Subsequently, all the error terms are extracted from the respective columns and are included in the unknown vector. Duplication of unknowns might occur due to these extractions. In the case of duplicated unknowns, the associated columns are merged to compact the system. The final system of equations is presented in Eq. (9).

$$\begin{pmatrix} 0 & 0 & \frac{4\tilde{w}_1}{L}-\frac{6\tilde{v}_2}{L^2} & \frac{6}{L^2} & \frac{2}{L} & -\frac{4}{L} & 0 & 0 & 0 & 0 & 0 & 0 & 0 \\ \frac{2}{L} & -\frac{1}{L} & 0 & 0 & 0 & 0 & 0 & 0 & 0 & 0 & 0 & 0 & 0 \\ 0 & 0 & \frac{12\tilde{v}_2}{L^3}-\frac{6\tilde{w}_1}{L^2} & -\frac{12}{L^3} & -\frac{6}{L^2} & \frac{6}{L^2} & \frac{12\tilde{v}_2}{L^3}+\frac{6\tilde{w}_3}{L^2} & -\frac{12}{L^3} & \frac{6}{L^2} & -\frac{6}{L^2} & 0 & 0 & 0 \\ 0 & 0 & \frac{2\tilde{w}_1}{L}-\frac{6\tilde{v}_2}{L^2} & \frac{6}{L^2} & \frac{4}{L} & -\frac{2}{L} & \frac{6\tilde{v}_2}{L^2}+\frac{2\tilde{w}_3}{L} & -\frac{6}{L^2} & \frac{4}{L} & -\frac{2}{L} & 0 & 0 & 0 \\ -\frac{1}{L} & \frac{1}{L} & 0 & 0 & 0 & 0 & 0 & 0 & 0 & 0 & 0 & 0 & 0 \\ 0 & 0 & 0 & 0 & 0 & 0 & \frac{6\tilde{v}_2}{L^2}+\frac{4\tilde{w}_3}{L} & -\frac{6}{L^2} & \frac{2}{L} & -\frac{4}{L} & 0 & 0 & 0 \\ -\frac{1}{L} & 0 & 0 & 0 & 0 & 0 & 0 & 0 & 0 & 0 & -1 & 0 & 0 \\ 0 & 0 & \frac{6\tilde{w}_1}{L^2}-\frac{12\tilde{v}_2}{L^3} & \frac{12}{L^3} & \frac{6}{L^2} & -\frac{6}{L^2} & 0 & 0 & 0 & 0 & 0 & -1 & 0 \\ 0 & 0 & 0 & 0 & 0 & 0 & -\frac{12\tilde{v}_2}{L^3}-\frac{6\tilde{w}_3}{L^2} & \frac{12}{L^3} & -\frac{6}{L^2} & \frac{6}{L^2} & 0 & 0 & -1 \end{pmatrix} \begin{pmatrix} EA_1u_2 \\ EA_2u_3 \\ EI_1 \\ EI_1\epsilon_{v2} \\ EI_1w_2 \\ EI_1\epsilon_{w1} \\ EI_2 \\ EI_2\epsilon_{v2} \\ EI_2w_2 \\ EI_2\epsilon_{w3} \\ H_1 \\ V_1 \\ V_3 \end{pmatrix} = \begin{pmatrix} M_1 \\ H_2 \\ V_2 \\ M_2 \\ H_3 \\ M_3 \\ 0 \\ 0 \\ 0 \end{pmatrix} \tag{9}$$

Step 5: **Generate all single unknowns and establish the constraints among coupled unknowns.** Identify all single unknowns in the new unknowns $\{z_e\}$, and the nonlinear constraints among them.

The existing unknown in Eq. (9) can be divided into two groups: (1) the coupled unknowns are in the form of the products of structural parameters and unknown displacements or error terms, such as $\{EA_1u_2,\ EA_2u_3,\ EI_1w_2,\ EI_2w_2,\ EI_1\varepsilon_{v2},\ EI_1\varepsilon_{w1},\ EI_2\varepsilon_{v2}$ and $EI_2\varepsilon_{w3}\}$; (2) the existing single unknowns include reactions $\{H_1, V_1, V_3\}$ and structural parameters θ (bending stiffnesses EI_1, EI_2). Apart from these two types of unknowns, the new unknown $\{z_e\}$ also includes single unknowns that are acquired from the coupled unknowns. These additional single unknowns contain the unmeasured displacements, (e.g. u_2, u_3 and w_2), the measurement errors, (e.g. ϵ_{w_1}, ϵ_{v_2} and ϵ_{w_3}) and structural parameters (EA_1, EA_2). Once different types of unknowns are determined, the equations that the coupled unknowns should equal the products of their relevant single unknowns (e.g. $EA_1u_2=EA_1 \cdot u_2$) are imposed as constraints during the optimization in Step 6.

Step 6: **Obtain the final estimation by minimizing Eq. (10)**. Solve the optimization problem with the objective function Eq. (10) and the nonlinear constraints obtained in step 5**.**

Despite the inclusion of the constraints (e.g. $EA_1u_2=EA_1 \cdot u_2$) among unknowns, the system of equations to be solved is always underdetermined. As a result, infinite solutions satisfy Eq. (9). To find the one with physical meaning from these solutions, it is always desirable to select the model minimizing the discrepancy between the measured and the predicted response. Hence, the objective function is to minimize the square sum of the ratios between the error term ϵ_{δ_i} and the associated measurements $\tilde{\delta}_i$, as presented in Eq. (10). N_m is the number of measured displacements.

$$f(z_e) = \sum_{i=1}^{N_m} \left(\frac{\epsilon_{\delta_i}}{\tilde{\delta}_i} \right)^2 \tag{10}$$

To improve the convergence and computation efficiency of the optimization, numerical scaling is applied such that the unknowns having widely varying orders of magnitude due to the physical nature are converted to be of similar orders. To do so, each column of the coefficient matrix B_e is scaled by the associated nominal values of the unknowns. The initial values for the error terms are zeros while those for the others are ones. No bound is applied to the estimated parameters, unless otherwise stated. Final estimations are obtained by multiplying the scaling factors with the solution from the optimization. All the aforementioned steps to implement the algorithm are summarized in Fig. 2.

2.4 Sensor placement

Apart from ensuring the observability of target parameters, the sensor placement should also consider the estimation accuracy. In structures of simple geometry or small number of Degrees Of Freedom (DOFs), experience or trial and error methods might be able to handle the task of sensor placement. However, this could be very challenging in complicated structures with many DOFs. One of the most known and commonly adopted approach for the optimal sensor placement was developed by Kammer[33]. This approach maximizes the information extracted from the measurement. This is achieved by maximizing the norm of the Fisher Information matrix [F] that is constructed from the modal and measurement covariance matrix. Since then, many variants of this method in SSI were proposed.

One Fisher Information matrix for the sensor placement in static SSI can be constructed from the noise variance and the gradient of structural displacements with respect to different structural parameters[3]. The sensor placement strategy used in this paper is developed based on this Fisher Information matrix. For an efficient unbiased estimation of $\hat{\theta}$, the lower bound of the covariance of estimations is given by the inversed Fisher Information matrix [F^{-1}]:

$$E\left[(\hat{\theta}-\theta)(\hat{\theta}-\theta)^T\right] \geq F^{-1} \tag{11}$$

The Fisher Information matrix $[F(\Theta)]$ contains the information about the values of the parameters θ based on the data from all measured locations[34]. Its formulation depends on the sensor location vector $\{\Theta\}$. The calculation of the matrix $[F(\Theta)]$ is shown by Eq. (12)

$$F(\Theta) = S(\Theta)^T \Psi_0^2 S(\Theta) \tag{12}$$

To calculate the Fisher Information matrix $[F(\Theta)]$, the sensitivity matrix $[S(\Theta)]$ for measured DOFs and the noise variance $\left[\Psi_0^2\right]$ are required. The matrix $[S(\Theta)]$ is the sensitivity matrix with respect to the sensor location vector $\{\Theta\}$. The vector $\{\Theta\}$ is a $3N_n \times 1$ Boolean vector $\{\Theta\}$. If the i^{th} DOF of the FEM is measured, the associated entry in $\{\Theta\}$ is one, otherwise zero.

Prior to obtain the sensitivity matrix $[S(\Theta)]$ for the measured DOFs, the sensitivity matrix $[S^a]$ for all DOFs is calculated by Eq. (13).

$$[S^a] = \frac{\partial \delta}{\partial \theta} = \frac{\partial [K(\theta)^{-1} f]}{\partial \theta} = \frac{\partial K(\theta)^{-1}}{\partial \theta} f = -K(\theta)^{-1} \frac{\partial K(\theta)}{\partial \theta} K(\theta)^{-1} f \tag{13}$$

The dimension of the sensitivity matrix $[S^a]$ is $3N_n \times N_p$. The element $S^a_{i,j}$, in the i^{th} row and j^{th} column of the matrix $[S^a]$, is the derivative of the i^{th} DOF with respect to the j^{th} parameter. The sensitivity matrix $[S(\Theta)]$ for the measured DOF is the collection of all those rows of $[S^a]$ where Θ_i equals one.

In estimation theory, the minimum variance in the estimations is desired, which means the minimization or maximization of some measures of [F]. Different norms of the matrix [F] have been used as the criteria for measuring the goodness of a measurement set regarding the estimation accuracy. These norms include the determinant, the trace and the minimum singular value of the matrix [F]. In this paper, the problem of sensor placement is formulated as the maximization of the determinant, *det*([F]), of the Fisher information matrix [F]. The i^{th} diagonal terms of the inversed matrix [F^{-1}] gives the lower bound of the variance of the estimations of the i^{th} parameter θ_i [35]. High values in the diagonal elements indicate that the estimations for the associated parameters have a high variation. Parameters of zones that are out of the load path cannot be identified accurately. This is manifested by the large diagonal elements related to these parameters in the inversed matrix [F^{-1}]. In this study, the threshold of 0.1 is used to differentiate between the identifiable and the unidentifiable parameters. The parameters associated with diagonal elements of [F^{-1}] that are less than 0.1 might be regarded as identifiable.

The sensor placement is a combinatorial problem whose dimension increases exponentially with the number of possible sensor locations. It is intractable to find the optimal solution by global search. However, some classic metaheuristic algorithms are competent in finding a near-optimal solution for the sensor placement problem[36]. The genetic algorithm is featured by bio-inspired operators such as mutation and crossover and selection. The discrete optimization problem arising from the sensor placement problem here is solved by the *Matlab* function *ga* with the objective function (14) and constraints (15)-(17).

$$\Theta_{\text{opt}} = \max_{\Theta} \det(F) \tag{14}$$

Subjected to

$$\sum_{i \in u} \Theta_i = N_{m,u} \quad \text{for any } i \text{ related to horizontal deflections } u \tag{15}$$

$$\sum_{i \in v} \Theta_i = N_{m,v} \quad \text{for any } i \text{ related to vertical deflections } v \tag{16}$$

$$\sum_{i \in w} \Theta_i = N_{m,w} \quad \text{for any } i \text{ related to rotations } w \tag{17}$$

$N_{m,u}$, $N_{m,v}$ and $N_{m,w}$ are the numbers of measured horizontal/vertical deflections and rotations, respectively.

3 Application in beam-like structures

To verify the effectiveness of the proposed method, a simply supported bridge example is analyzed here. Two cases are considered depending on the relation between the number of measured displacements, N_m, and the number of unknown parameters, N_p. In section 3.1, the performance of the MEMOM and the SSI by OM are compared when essential sets are used. In section 3.2, regarding the same structure, the performance of MEMOM and SSI by compatible OM [31] are compared when redundant sets are used. The considered factors include error levels, number of measurements, load cases.

3.1 Equivalence of MEMOM and SSI by OM in case of essential set

Assume an 18-m simply supported bridge with a concentrated load applied at one-third point, as shown in Fig. 3. The area and inertia of the girder are 0.1 m^2 and 0.015 m^4, respectively and the Young's modulus E is 210GPa. This structure is discretized into 18 elements each with the length of 1 m. Because the axial behavior of this structure is not excited under this load case, the identification of axial stiffness is not feasible. The parameterization of this model is shown in Fig. 3.

The systematic tools to find essential sets were proposed elsewhere[7,37]. To identify three bending stiffnesses, the essential sets should have three distributed measurements. One displacement is measured for each bending stiffness. Specifically, one from $\{v_2\text{-}v_7, w_1\text{-}w_7\}$, $\{v_7\text{-}v_{13}, w_7\text{-}w_{13}\}$ and $\{v_{13}\text{-}v_{18}, w_{13}\text{-}w_{19}\}$ for EI_1, EI_2 and EI_3, respectively. All potential essential sets are enumerated by taking one measurement from these sets. If duplicated measurements, e.g. w_7 or v_7, are detected, then that set is rejected. This leads to 2314 essential sets. 50 samples are generated for each set with an error level of 5%. One sample for a given measurement set is the collection of associated measurements generated by Eq. (18).

$$\tilde{\delta} = \delta \cdot (1 + E_{level} \cdot \xi) \tag{18}$$

Here, the measurements, $\tilde{\delta}$, are simulated by adding proportional errors to the theoretical values, δ, that are obtained by direct analysis. E_{level} is the error level in measurement and ξ is a random number following normal distribution with mean of zero and standard deviation of 0.5, same as in [31].

Regarding essential sets, it is always possible to find a set of parameters that exactly replicates any value of the measurement, either accurate or noisy measurements. In other words, the objective function (Eq. (10)) should be exactly zero. Regarding this simply supported bridge, 2314×50=115700 estimations are carried out. For all these estimations, the estimations from the MEMOM are capable

of replicating the noisy measurements. Hence, it is concluded that the proposed method and SSI by OM lead to the same estimation when essential sets are used. However, estimations from essential sets are far from satisfactory[28].

3.2 Comparison of the performance of different methods in a beam-like structure

In order to improve the estimation accuracy, redundant sets are used. In beam-like structures, the explicit expression of the compatibility conditions can be found symbolically. In this section, the performance of the SSI by compatible OM and the MEMOM is compared for the structure depicted in Fig. 3 regarding different factors. The controlled factors are the number of measurements, N_m, and the error levels, $E_{level,}$ and the load cases while the parameterization is still the same

(1) Effect of curvatures

In the first comparison, the load case is a vertical load applied at node 7. Three measurement sets are used, including (1) Set 1 (v_3, v_5, v_7, v_9, v_{11}, v_{13}, v_{15} and v_{17}); (2) Set 2 (v_3-v_5, v_7, v_9-v_{11}, v_{13} and v_{15}-v_{17}) and (3) Set 3 (v_2-v_{17}). These sets are the same as those in previous study[31]. The error levels range from 1% to 5%. 2000 samples are generated for each measurement set at all error levels using Eq. (17). In this paper, all the estimations are normalized by their real values, unless otherwise stated. To evaluate the performance of different algorithms, Eqs. (19)-(21) are used.

$$\hat{\theta}_m = \frac{\Sigma_{i=1}^{N_s} \hat{\theta}_{i,r}}{N_s} \tag{19}$$

$$\hat{\theta}_{sd} = \sqrt{\frac{1}{N_s - 1} \Sigma_{i=1}^{N_s} \left(\hat{\theta}_{i,r} - \hat{\theta}_m\right)^2} \tag{20}$$

$$\hat{\theta}_{COV} = \frac{\hat{\theta}_{sd}}{\hat{\theta}_m} \tag{21}$$

Here, $\hat{\theta}_{i,r}$ is the estimation (normalized by the real value) of parameter θ using the i^{th} sample. N_s is the number of samples. $\hat{\theta}_m$ is the mean of all the N_s estimations of θ. The closer the mean, $\hat{\theta}_m$, to one, the lower the bias. In addition, $\hat{\theta}_{COV}$ describes the variability among all the N_s estimations of θ.The smaller the $\hat{\theta}_{COV}$, the less variation in the estimations of θ.

In this example (Fig. 3), the target parameters are EI_1-EI_3. A careful examination shows that both methods lead to the same estimations for each measurement set and each error level. The results are presented as the bar graph with error bar in Fig. 4a. The bar graph shows the mean of the estimations while the error bar indicates one standard deviation of the estimations.

As the load is applied at node 7, the elements associated with EI_1 and EI_2 are more excited than those associated with EI_3. From Fig. 4a, it is seen that the standard deviation, which is the length of the error bar, increases much faster in zones of less excited zones (EI_3). The bias of the estimations of EI_1-EI_3 is small. The worst case is an overestimation of 1.45% in EI_3 with an error level of 5%. However, it should be pointed out that the bias also increases faster in less excited zones.

(2) Effect of loading cases

The performance of the two methods is also compared using different load cases with set 1 (v_3, v_5, v_7, v_9, v_{11}, v_{13}, v_{15} and v_{17}) and an error level of 5%. The load moves from V_2 through V_{10}, leading to 9 load cases. Under each load case, the estimations produced by the proposed method are the same as

those obtained via SSI by compatible OM. The results are presented in Fig. 4b. When load changes from V_2 to V_{10}, the curvatures for areas associated with EI_1 decreases and the standard deviation of the estimations of EI_1 increase correspondingly. An opposite trend is observed for the parameter EI_3. In addition, the estimations of EI_1 and EI_3 have the same mean and standard deviation when identical curvatures are excited in areas associated with these two parameters in the load case of V_{10}.

The same performance of the two methods might be due to the fact that the inclusion of the nonlinear constraints among the unknowns in the proposed method implicitly contains the compatibility conditions (the geometrical relations that the displacements should satisfy). Hence, it is concluded that: (1) the proposed method is applicable in beam-like structures and (2) its accuracy is as good as the SSI by compatible OM. For clarity, the difference of the mentioned methods is summarized in Table. 1.

4 Application of the proposed method in frame structures

Due to the coupling of the bending and the axial behaviors in frames or inclined beams, obtaining compatibility conditions in such structures is nontrivial. However, the proposed method does not suffer from this limitation. In this section, the effectiveness of the proposed method is verified in two examples. The first example corresponds to a floor beam (see dashed ellipse in Fig. 5a) in a 13-story frame building adapted from previous research[4] while the second example corresponds to a rigid frame bridge with inclined piers.

4.1 Example 1: Floor beam in a frame

Damage in structural members that have insignificant contribution to the structural response under the given load case cannot be accurately identified[3]. Simultaneous identification of all parameters requires a well-designed loading scheme capable of exciting all structural members sufficiently. On the other hand, many sensors are required for data collection. These might not be feasible in real life for technical and economic reasons. Hence, it is more interesting to identify the parameters of a local area because only a small zone needs to be excited and the number of sensors is significantly reduced.

In the following study, the focus is to identify the parameters of a floor beam on 3rd floor using noisy measurements. The elastic moduli is 3.5×10^4 MPa. Geometrical properties for different elements are provided in Table 2. In previous study, the floor beams were assumed to have constant stiffness and measurement errors were not included[4]. In this study, the real values of the parameters for the target floor beam are the same as those in element type VIII. However, different parameterizations are applied for this beam (Fig. 5b) and these parameters are assumed different and unknown. An error level of 5% is also included in the numerical analysis. The effect of curvatures in different zones of the floor beam is investigated first. Subsequently, the benefit of including rotations in the measurement set is illustrated. At the end of section 4.1, different constraints limiting the feasible values of the unidentifiable parameters are compared.

(1) Effect of curvatures

The analyzed floor beam is evenly discretized into 42 elements. To show the effect of curvatures, four scenarios (Table 3 and Fig. 5b) are studied regarding two load cases and two parameterizations of this floor beam. The coarse parameterization models the structure with three bending stiffnesses, EI_{1c}-EI_{3c}. Each parameter is related to fourteen elements. The fine parameterization models the structure with seven bending stiffnesses, EI_{1f}-EI_{7f}. Each parameter is related to six elements. The load

case 1 (LC1) is a uniform load of 25kN/m applied along the entire span while the load case 2 (LC2) is of the same magnitude but only applied on the left four elements (2.667 m). The configuration and the associated moment diagrams are depicted in Fig. 5b. The bending behaviors for the zones of EI_{2f} and EI_{6f} are not quite excited under LC1 (scenario 3). Similar situation is observed for the zones of EI_{4f}-EI_{7f} under LC2 (scenario 4). In scenarios 1 and 2, though the inflection points are included in zones related to EI_{1c} and EI_{3c}, the bending behavior for these zones is still sufficiently excited due to the wide coverage of the zones associated with EI_{1c} and EI_{3c}. Note that the number, the location and the type of measurements affect the result of the estimations. Providing that the number of measurements is three times the number of parameters, $N_m=3N_p$, and at least half of these measurements are composed of deflections, the near-optimal measurement set for each scenario is determined by the method in section 2.4.

According to the diagonal terms in the associated inversed Fisher Information matrix, EI_{2f} and EI_{6f} in scenario 3 and EI_{5f}-EI_{7f} in scenario 4 cannot be accurately identified. Hence, they are excluded from the objective function and the absolute constraint of [0, 10] are applied to limit the feasible range of these unidentifiable parameters. 500 samples are generated for each scenario with an error level of 5% using Eq. (17). The mean and standard deviation are summarized as the bar graph with error bar in Fig. 6.

When the number of measurements, N_m, is three times the number of parameters, N_p: (1) N_m=9 measurements are sufficient to provide unbiased and robust estimations of EI_{1c}-EI_{3c} in both load cases. However, larger variations in EI_{2c} and EI_{3c} are observed for LC2 than those for LC1. This is due to the fact that the curvature in zones of EI_{2c} and EI_{3c} is much less excited in LC2 than that in LC1. A slight underestimation of EI_{3c} is also observed in LC2. (2) This phenomenon is more noticeable in Fig. 6b. N_m=21 measurements are used to estimate 7 parameters in the fine parameterization. As expected, the estimations of EI_{2f} and EI_{6f} from LC1 have large bias and variations. Note that the bending behavior for zones of EI_{2f} in LC2 are well excited. Comparing the estimations of EI_{2f} from LC1 and LC2, the latter one is more consistent and less variable. As expected, the estimations of EI_{5f}-EI_{7f} from LC2 are not reliable. (3) Comparing Figs. 6a and 6b, it is seen that the estimations of bending stiffnesses for the coarse parameterization is much better than those for the fine parameterization regarding the unbiasedness and variation under the same load case.

In order to improve the estimations of the parameters associated with null curvature zones, two more sets with numerous measurements are investigated for the case of fine parameterization. The first set is to measure the deflection and the rotation every 2 nodes, leading to 42(=6N_p) measurements with the deflections at the joint excluded. The second one is to measure the deflection and the rotation of each node, leading to 84(=12N_p) measurements with the deflection at the joint excluded. The results are also summarized in Fig. 6b. Despite the improvement in all estimations, the standard deviations in the estimations of parameters associated with null curvature zones are still large and thus unreliable.

(2) Type of measurements

It was shown that using rotations had theoretical advantages when estimating the parameters. Wide applications of inclinometers in real engineering practice are also provided. The effect of including different number of rotations with a fixed number of measurements on the estimations is studied here. The load case is LC1 and the parameterization is the fine one, as seen in the scenario 3 in Fig. 5b. The number of measurements N_m is 25. The number of rotations varies from 0 to 25, adding up to 26 measurement sets. For each set, the near-optimal measurement set is found by Fisher Information matrix. 500 estimations are obtained for each set using the same setting in section 4.1. The result is summarized in Fig. 7. It is found that using rotations cannot improve the estimations of parameters

associated with null curvature zones in this structure. Hence, the results for EI_{2f} and EI_{6f} are not presented.

When no rotation is used, the bias in EI_{3f} and EI_{5f} is 32.0% and 64.3%, respectively. The extent of the bias in EI_{3f} and EI_{5f} decreases with the number of rotations. It should be noted that the inclusion of one rotation in the measurements reduces the bias significantly. In addition, the deviations of the mean of the estimations for all parameters are always within 1.0% when the number of rotations exceeds 8. Regarding the COV of the estimations, a gradual decrease is observed when the number of rotations increases from 0 to 17. However, the COVs of the estimations for all parameters do not improve noticeably when more rotations are used.

From this analysis, it is seen that: (1) Compared with using only deflections, the inclusion of rotations in the measurements improves the estimations remarkably with respect to the unbiasedness and the extent of variation; (2) The rate of improvement due to the inclusion of rotations is drastic initially. When the number of rotations reach a certain number, this rate becomes slow, as indicated by the plateau in Fig. 7b.

(3) Effect of different constraints to limit the value of the estimates in the null curvature zones

The load path by one load case can hardly cover each part of a local region, as depicted by the moment diagrams in Fig. 5b. The parameters for unexcited members may not be accurately identified without using multiple load cases. This is justified by the observation that either increasing the number of measurements or including rotations cannot improve the estimations for parameters associated with null curvature zones using only one load case. However, multiple load cases might be costly, cumbersome and hence not desirable for engineers. Providing that only one load case is used, it is interesting to limit the feasible ranges of those unidentifiable parameters by imposing different types of constraints during the estimation process. In this section, the effect of these constraints on the unbiasedness and the variation of the estimations for those identifiable parameters are investigated.

In previous study, the absolute constraint that $EI_i \in [0, 10]$ is imposed on unidentifiable parameters, for instance, EI_{2f} and EI_{6f} in LC1. Two types of constraints are studied here. The first type is related to a tight absolute constraint of [0.5, 1.5] on those unidentifiable parameters. The second type is a relative constraint that the parameters for the null curvature zones are between those for adjacent zones. This is to say, $(EI_{2f}\text{-}EI_{1f})$ $(EI_{2f}\text{-}EI_{3f})\leq 0$ and $(EI_{6f}\text{-}EI_{5f})$ $(EI_{6f}\text{-}EI_{7f})\leq 0$. The load case, the parameterization and the measurement sets are the same as scenario 3 in Fig. 5b. It should be pointed out that the following discussions will focus on the results of those identifiable parameters (EI_{1f}, EI_{3f}-EI_{5f}, EI_{7f}) in this scenario.

Under both types of constraints, 500 estimations are carried out for each measurement set using the identical data in section 4.2. For both types of constraints, the mean and the COVs are summarized in Fig.8a and 8b, respectively.

Regarding the tight absolute constraint, the bias and the COVs for EI_{3f} and EI_{5f} are not always satisfactory when the number of rotations used is less than 5. For instance, when 4 rotations are used, the bias in EI_{3f} is 3.5% and the COVs is 0.11. Hence, the results of using less than 5 rotations are not included in this figure. When the number of rotations is equal to or greater than 5: (1) the bias in all identifiable parameters is always less than 1.0%. (2) The bias decreases with the number of rotations. (3) The bias in EI_{3f} is the lowest among the bias for all parameters because the bending behavior of the local zone associated with EI_{3f} is fully excited.

In the case of relative constraints, the bias in EI_{3f} is also the lowest one. However, bias of around 1-2% exists in those estimations for parameters associated with regions adjacent to null curvature zones. In Fig.8a, it is observed that the bias in EI_{1f} and EI_{3f} are very close in magnitude but different in sign. This might be due to the fact that introducing the relative constraints averages the estimations of EI_{1f}, EI_{2f} and EI_{3f}. Similar phenomenon is observed for parameters EI_{5f} and EI_{7f}.

Regarding the variation of the estimations, the COVs for those identifiable parameters can be reduced by both types of constraints. The COVs for EI_{1f}, EI_{3f}-EI_{5f}, EI_{7f} obtained from the tight absolute constraint [0.5, 1.5] are always lower than those respective ones obtained from the constraint [0, 10] for all measurement sets. These COVs drop more significantly when the relative constraint is imposed. The comparison of COVs obtained from the tight absolute constraint and the relative one is depicted in Fig. 8b.

The analysis of the comparison between the results obtained from the absolute constraint and the relative constraint shows that: (1) when insufficient rotations are introduced in the measurement set, biased estimations can be obtained despite of the constraints imposed on the parameters of insufficiently excited zones. (2) When sufficient rotations are introduced, both the tight and the relative constraints can reduce the variations of the estimations for those identifiable parameters where the bending behavior are sufficiently excited. (3) The relative constraint reduces the variations more than the tight absolute constraint at the cost of slight bias.

4.2 Example 2: A rigid frame bridge with inclined piers

The effect of including rotation measurements is studied in the rigid frame bridge with inclined piers. The decks of this bridge are subjected to a uniform load of 24kN/m. The FEM of this structure and its parameterization is depicted in Fig.9a. The elastic modulus is same as in the previous example. The area and the inertia of the deck are $4m^2$ and $2.6m^4$ while those for the deck are $3m^2$ and $0.88m^4$. Under this loading case, the axial stiffnesses EA_1-EA_6 cannot be identified due to the fact that the axial behaviors of the decks are not excited. Hence, the target parameters include the bending stiffnesses (EI_1-EI_6) of the decks, the bending stiffnesses (EI_7-EI_{10}) and the axial stiffnesses (EA_7-EA_{10}) of the inclined piers. It should be noted that both the axial behaviors and the bending behaviors of the piers lead to horizontal and vertical movement of the whole structure.

To study the effect of including rotations on the estimation accuracy of these 14 parameters, the results of 20 measurement sets are compared. Each set has 24 measurements in total when the number of horizontal deflections is five and the number of rotations varies from 0 to 19. The measurement configuration for the case of 9 rotations is depicted in Fig. 9b.

For each measurement set, 500 samples are generated and an error level of 5% is included. The mean and the COV of the estimations for different measurement sets are calculated. Despite the coupling of bending and axial stiffnesses of the piers, all parameters are well identified with a maximum deviation of less than 1% in each measurement set. The COVs of the estimations of parameters for the decks and the piers are presented in Fig. 10a and 10b, respectively.

From Fig.10a and 10b, it is seen that when no rotation is used, large variations are observed for both bending stiffnesses of decks and piers. When the number of rotations increases, the variations of the bending stiffnesses for both the decks and the piers get smaller and becomes stable when the number of rotations is more than 9, which is similar to the conclusion in section 4.2. In Figure 10b, it is observed that the COVs for the estimations for the axial stiffnesses (EA_7-EA_{10}) of the piers are not

sensitive to the number of rotations. The COVs for EA_8 and EA_9 are around 0.040 while those for EA_7 and EA_{10} are around 0.017.

From this analysis, it is seen that: (1) The inclusion of rotations in the measurements improves the estimations remarkably with respect to the extent of variation; (2) The rate of improvement due to the inclusion of rotations is drastic initially. When the number of rotations reach a certain number, this rate becomes slow; (3) The axial stiffnesses of the piers are not sensitive to the number of rotations.

5 Conclusion

This paper proposes a measurement error-minimizing observability method for the static structure system identification. For the first time in the literature, to deal with the biasedness in the estimations, those error terms in the coefficient matrix of the observability equations are separated and moved into the unknowns. The resulting equations are solved by minimizing the square sum of the ratios between the error terms and the associated measurements subjected to the nonlinear constraints among the unknowns.

The proposed method is first validated in a beam-like structure with previous methods using essential sets and redundant sets. The method leads to identical results in all cases. This might be due to the fact that the geometrical relations among displacements are implicitly imposed by the nonlinear constraints in the proposed method.

In structures where axial and bending behaviors are coupled, the SSI by compatible OM cannot be applied. The applicability of MEMOM is shown by a frame structure and a rigid frame bridge. In the frame structure, the identification of a floor beam is investigated regarding the effect of curvatures, the measurement types and the constraint on those unidentifiable parameters. The results indicate that the accuracy of the estimation of a given parameter θ highly depends on the curvature of the zones of parameter θ, which is related to the parameterization and the load case of the structure. In the case of coarse parameterization, the bending behavior for all zones are sufficiently excited in both load cases, hence the estimations for all parameters are satisfactory. In the case of fine parameterization, the parameters for more excited zones are estimated much more accurately than those for less excited zones. The estimations of the parameters for null curvature zones are greatly biased and variable. Including plentiful measurements cannot improve the estimation accuracy for parameters associated with null curvature zones. To investigate the effect of measurement type, the estimations from 26 measurement sets are evaluated regarding different number of rotations. The analysis of these simulations shows that the inclusion of rotations in measurements is critical for accurate estimations. As the number of rotations increases, the improvement in the estimations is significant initially but reaches a plateau at a given moment. The inclusion of rotations cannot solve the issue of bad estimations of parameters associated with null curvature zones in frame structures. Providing only one load case is used, the effect of limiting the feasible range of the estimations for parameters of null curvature zones is studied in the frame example. It is found that: (1) To obtain unbiased and robust estimations, the inclusion of rotations in the measurement set is necessary despite different types of constraints. (2) The variations for parameters for zones whose curvatures are well excited can be reduced when tight absolute constraints or relative constraints are imposed on the estimations of parameters associated with null curvature zones. (3) The relative constraint reduces the variations more than the tight absolute constraint at the cost of slight bias.

The rigid frame bridge example proves the applicability of the proposed method in identifying parameters for inclined elements. The importance of the inclusion of rotation measurements is also

demonstrated. When the number of rotations increases, significant improvement of the estimations is observed for most of the parameters. The importance of rotation measurements should be emphasized in the static SSI.

Acknowledgement

This work was partially funded by the Spanish Ministry of Economy and Competitiveness and the FEDER fund through the grant project (BIA2013-47290-R) directed by Jose Turmo. It is also to be noted that part of this work was done through a collaborative agreement between Tongji University (China) and Technical University of Catalonia, UPC, BarcelonaTech. This included an exchange of faculty financed by the High-End Foreign Experts program (GDW20143100115) from Chinese Government. Funding for this research has been provided to Mr. Lei Jun by the Chinese Scholarship Council through its program (201506260116) and by the Spanish Ministry of Economy and Competitiveness through its program (BES-2014-07022) for his PhD stays.

Reference

1. Castillo E, Lozano-Galant JA, Nogal M, Turmo J. New tool to help decision making in civil engineering. *J Civ Eng Manag*. 2015;21(6):689–97.
2. Shahsavari V, Chouinard L, Bastien J. Wavelet-based analysis of mode shapes for statistical detection and localization of damage in beams using likelihood ratio test. *Eng Struct*. 2017;132:494–507.
3. Bakhtiari-Nejad F, Rahai A, Esfandiari A. A structural damage detection method using static noisy data. *Eng Struct*. 2005;27(12 SPEC. ISS.):1784–93.
4. Lozano-Galant JA, Nogal M, Castillo E, Turmo J. Application of observability techniques to structural system identification. *Comput Civ Infrastruct Eng*. 2013;28(6):434–50.
5. Sheena Z, Unger A, Zalmanovich A. Theoretical stiffness matrix correction by using static test results. *Isr J Technol*. 1982;20:245–53.
6. Banan MR, Banan MR, Hjelmstad KD. Parameter Estimation of Structures from Static Response. I. Computational Aspects. *J Struct Eng*. 1994;120(11):3243–58.
7. Lei J, Nogal M, Lozano-Galant JA, Xu D, Turmo J. Constrained observability method in static structural system identification. *Struct Control Heal Monit*. 2018;25(1):2040e.
8. Tomàs D, Lozano-Galant JA, Ramos G, Turmo J. Structural system identification of thin web bridges by observability techniques considering shear deformation. *Thin-Walled Struct*. 2018;123:282–93.
9. Ghrib F, Li L, Wilbur P. Damage Identification of Euler –Bernoulli Beams using static response. *J Eng Mech*. 2012;138(5):405–15.
10. Sanayei M, Phelps JE, Sipple JD, Bell ES, Brenner BR. Instrumentation, Nondestructive Testing, and Finite-Element Model Updating for Bridge Evaluation Using Strain Measurements. *J Bridg Eng*. 2012;17(2):130–8.
11. Choi I-Y, Lee JS, Choi E, Cho H-N. Development of elastic damage load theorem for damage detection in a statically determinate beam. *Comput Struct*. 2004;82(29):2483–92.
12. Abdo MA-B. Parametric study of using only static response in structural damage detection. *Eng Struct*. 2012;34:124–31.
13. Boumechra N. Damage detection in beam and truss structures by the inverse analysis of the static response due to moving loads. *Struct Control Heal Monit*. 2017;24(10):1–10.
14. Sun Z, Nagayama T, Nishio M, Fujino Y. Investigation on a curvature-based damage detection method using displacement under moving vehicle. *Struct Control Heal Monit*. 2017;e2044.

15. Li Z, Park HS, Adeli H. New method for modal identification of super high-rise building structures using discretized synchrosqueezed wavelet and Hilbert transforms. *Struct Des Tall Spec Build*. 2017;26(3):e1312.
16. Jin SS, Jung HJ. Sequential surrogate modeling for efficient finite element model updating. *Comput Struct*. 2016;168:30–45.
17. Astroza R, Nguyen LT, Nestorović T. Finite element model updating using simulated annealing hybridized with unscented Kalman filter. *Comput Struct*. 2016;177:176–91.
18. Al-Hussein A, Haldar A. Unscented Kalman filter with unknown input and weighted global iteration for health assessment of large structural systems. *Struct Control Heal Monit*. 2016;23(1):156–75.
19. Ismail Z, Abdul Razak H, Abdul Rahman AG. Determination of damage location in RC beams using mode shape derivatives. *Eng Struct*. 2006;28(11):1566–73.
20. Ciambella J, Vestroni F. The use of modal curvatures for damage localizationin beam-type structures. *J Sound Vib*. 2015;340:126–37.
21. Yang Q, Sun B. Structural damage localization and quantification using static test data. *Struct Heal Monit*. 2010;10(4):381–9.
22. Andreaus U, Baragatti P, Casini P, Iacoviello D. Experimental damage evaluation of open and fatigue cracks of multi-cracked beams by using wavelet transform of static response via image analysis. *Struct Control Heal Monit*. 2017;24(4):1–16.
23. Wei Z, Qin C, Cai L, Zhu S, Chen ZW, Cai QL, et al. Damage quantification of beam structures using deflection influence lines. *Struct Control Heal Monit*. 2018;25(June):1–17.
24. Park HS, Shin Y, Choi SW, Kim Y. An integrative structural health monitoring system for the local/global responses of a large-scale irregular building under construction. *Sensors*. 2013;13(7):9085–103.
25. Liu T, Yang B, Zhang Q. Health Monitoring System Developed for Tianjin 117 High-Rise Building. *J Aerosp Eng*. 2017;30(2):1–13.
26. Sousa H, Cavadas F, Henriques A, Bento J, Figueiras J. Bridge deflection evaluation using strain and rotation measurements. *Smart Struct Syst*. 2013;11(4):365–86.
27. Zhang W, Sun LM, Sun SW. Bridge-Deflection Estimation through Inclinometer Data Considering Structural Damages. *J Bridg Eng*. 2017;22(2):04016117.
28. Lei J, Lozano-Galant JA, Nogal M, Xu D, Turmo J. Analysis of measurement and simulation errors in structural system identification by observability techniques. *Struct Control Heal Monit*. 2017;24(6):1–21.
29. M SF, Antonio V. Digital Control Engineering:Analysis and Design. 2nd ed. Academic Press; 2013.
30. Castillo E, Conejo AJ, Eva Pruneda R, Solares C. Observability in linear systems of equations and inequalities: Applications. *Comput Oper Res*. 2007;34(6 SPEC. ISS.):1708–20.
31. Lei J, Xu D, Turmo J. Static structural system identification for beam-like structures using compatibility conditions. *Struct Control Heal Monit*. 2018;25(1):e2062.
32. Nogal M, Lozano-Galant JA, Turmo J, Castillo E. Numerical damage identification of structures by observability techniques based on static loading tests. *Struct Infrastruct Eng*. 2015;12(9):1216–27.
33. Kammer DC. Sensor Placement for On-Orbit Modal Identification and Correlation of Large Space Structures. *J Guid Control Dyn*. 1991;14(2)(August):251–9.
34. Guo YL, Ni YQ, Chen SK. Optimal sensor placement for damage detection of bridges subject to ship collision. *Struct Control Heal Monit*. 2017;24(9):1–16.
35. Sanayei M, Dicarlo CJ, Rohela P, Miller EL, Kilmer ME. Sensor Placement using Fisher Information Matrix for Robust Finite Element Model Updating. *Life Cycle Reliab Saf Eng*. 2015;4(2):28–39.
36. Hou R, Xia Y, Xia Q, Zhou X. Genetic algorithm based optimal sensor placement for L1-regularized damage detection. *Struct Control Heal Monit*. 2018;(September 2018):1–14.

37. Lozano-Galant JA, Nogal M, Turmo J, Castillo E. Selection of measurement sets in static structural identification of bridges using observability trees. *Comput Concr*. 2015;15(5):771–94.

Captions:

Fig. 1. A 3-node simply supported beam with measurement set (w_1, v_2 and w_3)

Fig. 2. Flow chart of the proposed algorithm.

Fig. 3. A 19-node simply supported beam with three target parameters (bending stiffnesses EI_1-EI_3)

Fig. 4. Bar graph with error bar for the estimations of EI_1-EI_3: (a) under the load case of V_7 with different error levels; (2) under different load cases (V_2-V_{10}) with an error level of 5%.

Fig. 5. (a) Finite element model for the 13-story frame (b) Four scenarios for the identification of the floor beam (different load cases, parameterizations and moment diagrams)

Fig. 6. The bar graph with error bar for the estimations of parameters in (a) scenarios 1 and 2; (b) scenarios 3 and 4. (The legend indicates the load case and the number of measurements, respectively. Subscript *f* and c indicate fine and coarse parameterization, respectively. N_p, number of parameters).

Fig.7. Using different number of rotations: (a) Mean (b) Coefficient Of Variation (COV)

Fig. 8. Estimations using different number of rotations with the absolute constraint of [0.5, 1.5] (triangle) and the relative constraint (dot): (a) Mean (b) Coefficient Of Variation (COV)

Fig.9 (a) Finite element model and the parameterization of the rigid frame bridge; (b) measurement set of 5 horizontal deflections, 10 vertical deflection and 9 rotations.

Fig.10 The Coefficients of Variation for the parameters of (a) the decks (EI_1-EI_6); (b) the piers (EA_7-EA_{10}，EI_7-EI_{10}).

Table. 1 Characteristic of different observability method

Method	Applicability	Optimization involved	Nonlinear constraints	Objective function	Sensitive to errors
SSI by OM[32]	Beam-like/ frame	No	-	-	Yes
SSI by constrained OM[7]	Beam-like/ frame	Yes	Yes	Force Residues	Yes
SSI by compatible OM [31]	Beam-like	Yes	No	Displacement Residues	No
SSI by MEMOM	Beam-like/ frame	Yes	Yes	Displacement Residues	No

Table 2. Geometrical properties for different elements

Element type	Area (m^2)	Inertia (m^4)
I	0.563	0.026
II	0.360	0.011
III	0.250	0.005
IV	0.360	0.011
V	0.250	0.011
VI	0.160	0.002
VII	1.800	5.400
VIII	0.180	0.005

Table 3. Description of different scenarios

Scenarios	Parameterization	Load case
1	Coarse, three parameters	Uniform load over whole span
2	Coarse, three parameters	Uniform load on the left
3	Fine, seven parameters	Uniform load over whole span
4	Fine, seven parameters	Uniform load on the left

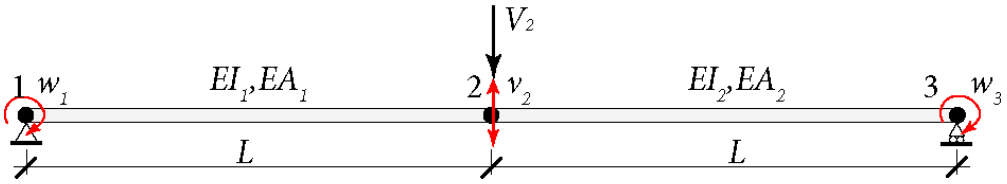

Fig. 1. A 3-node simply supported beam with measurement set (w_1, v_2 and w_3).

79x14mm (300 x 300 DPI)

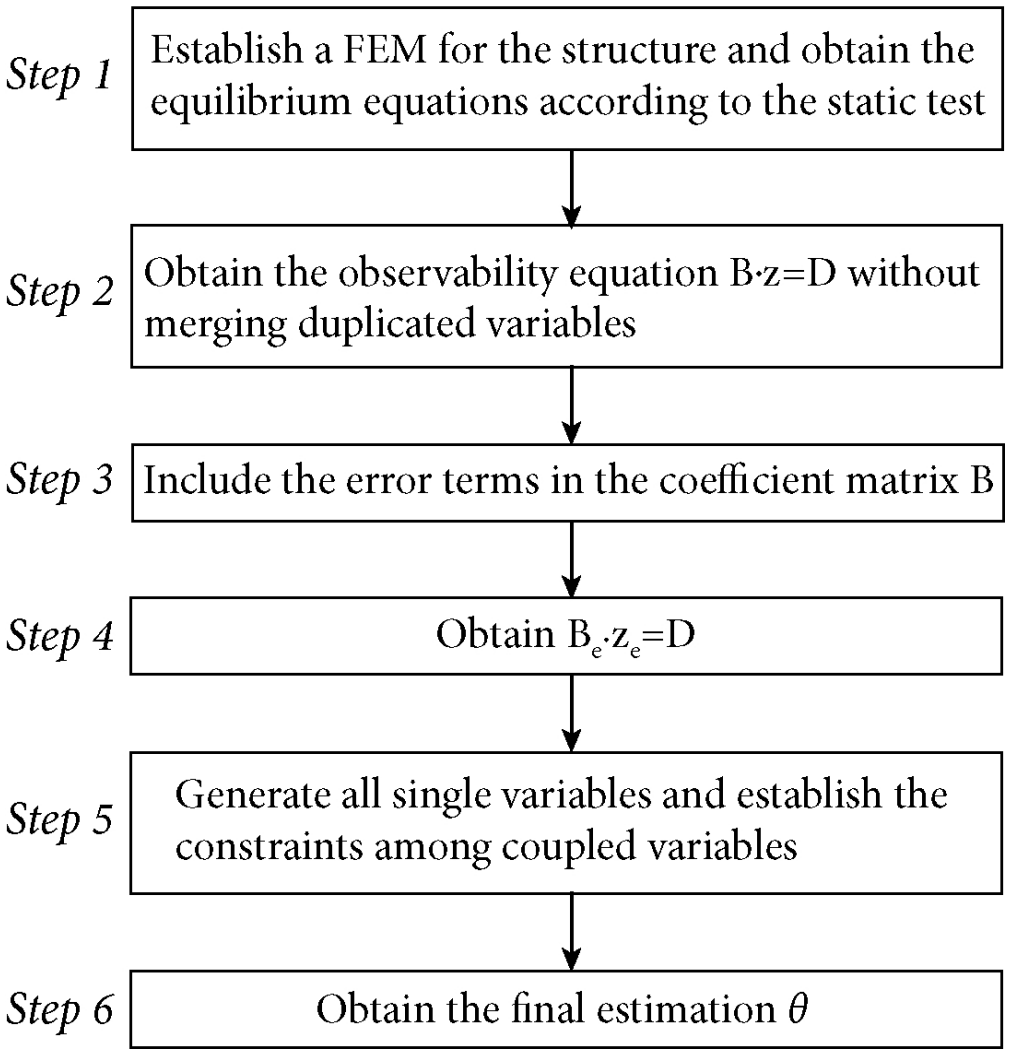

Fig. 2. Flow chart of the proposed algorithm.

91x96mm (300 x 300 DPI)

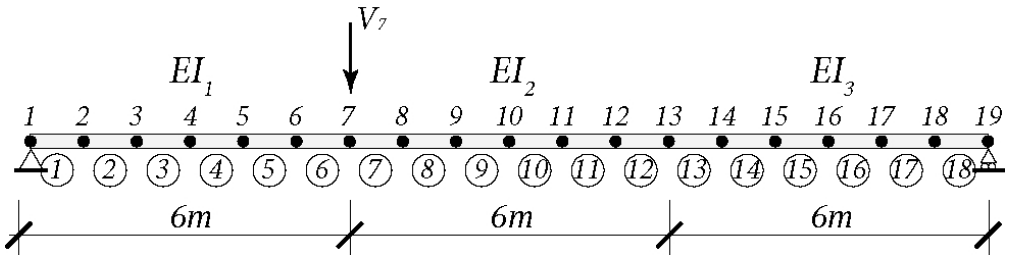

Fig. 3. A 19-node simply supported beam with three target parameters (bending stiffnesses EI_1-EI_3).

82x20mm (300 x 300 DPI)

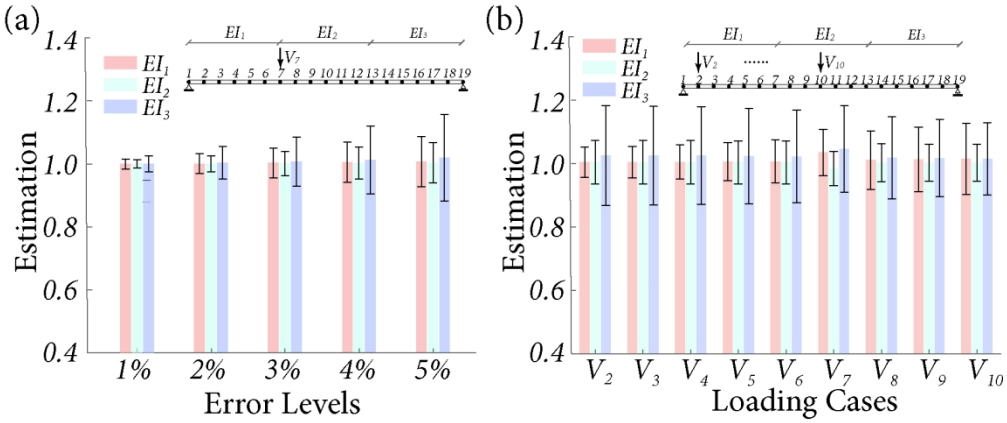

Fig. 4. Bar graph with error bar for the estimations of EI_1-EI_3: (a) under the load case of V_7 with different error levels; (2) under different load cases (V_2-V_{10}) with an error level of 5%.

153x64mm (300 x 300 DPI)

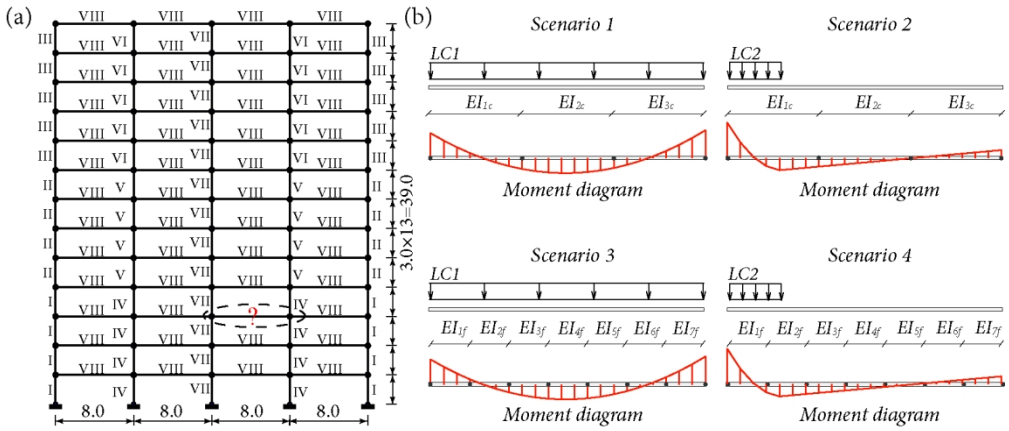

Fig. 5. (a) Finite element model for the 13-story frame; (b) Four scenarios for the identification of the floor beam (different load cases, parameterizations and moment diagrams)

149x63mm (300 x 300 DPI)

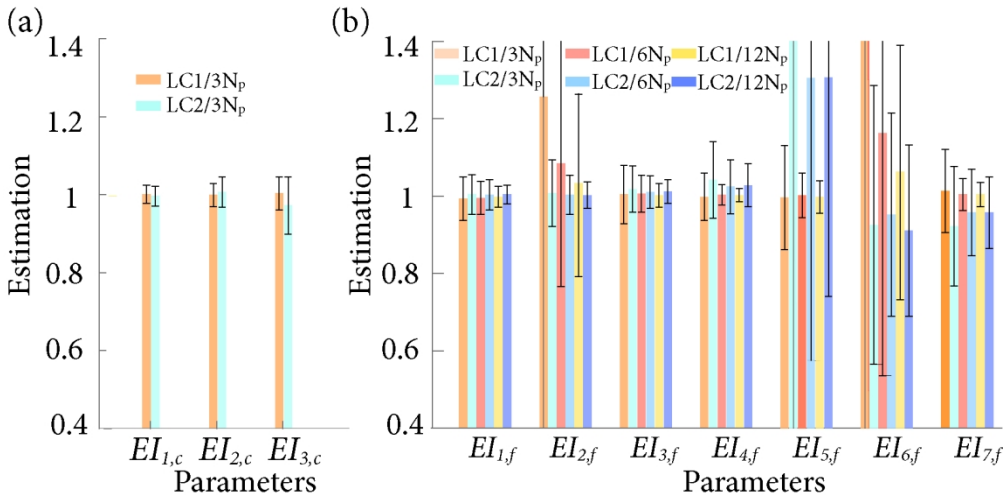

Fig. 6. The bar graph with error bar for the estimations of parameters in (a) scenarios 1 and 2; (b) scenarios 3 and 4. (The legend indicates the load case and the number of measurements, respectively. Subscript *f* and *c* indicate fine and coarse parameterization, respectively. N_p, number of parameters).

154x76mm (300 x 300 DPI)

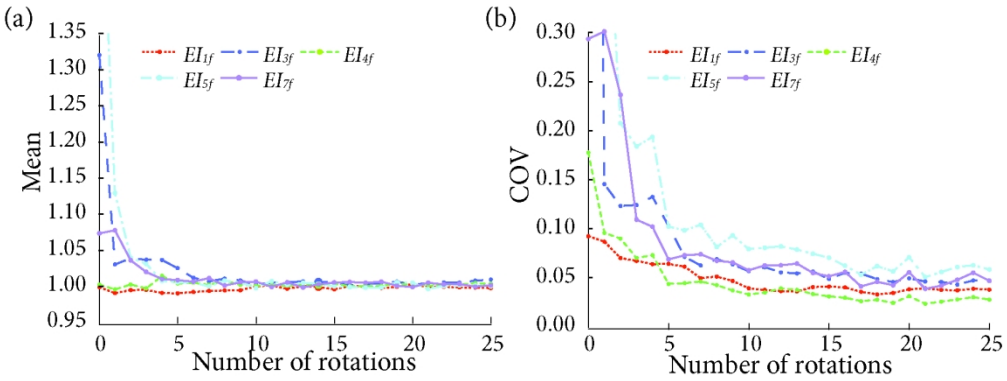

Fig.7. Using different number of rotations: (a) Mean (b) Coefficient Of Variation (COV)

162x61mm (300 x 300 DPI)

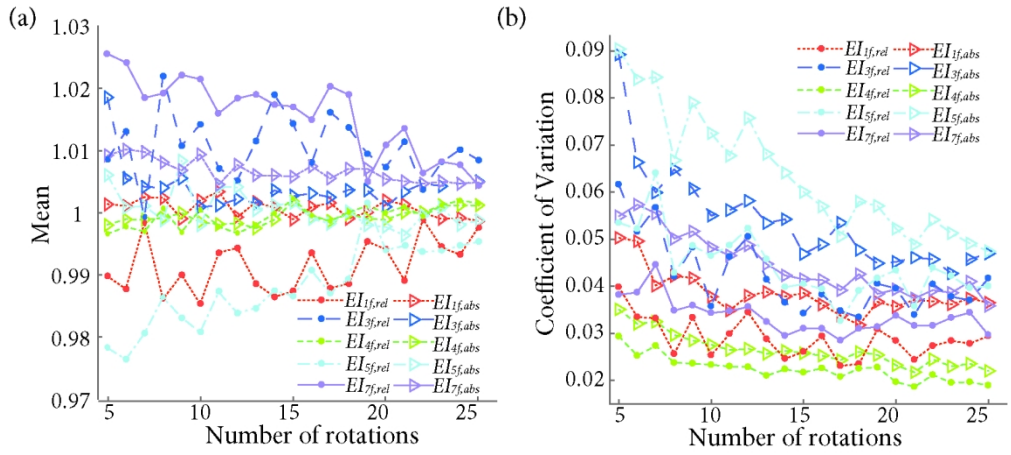

Fig. 8. Estimations using different number of rotations with the absolute constraint of [0.5, 1.5] (triangle) and the relative constraint (dot): (a) Mean (b) Coefficient Of Variation (COV)

150x67mm (300 x 300 DPI)

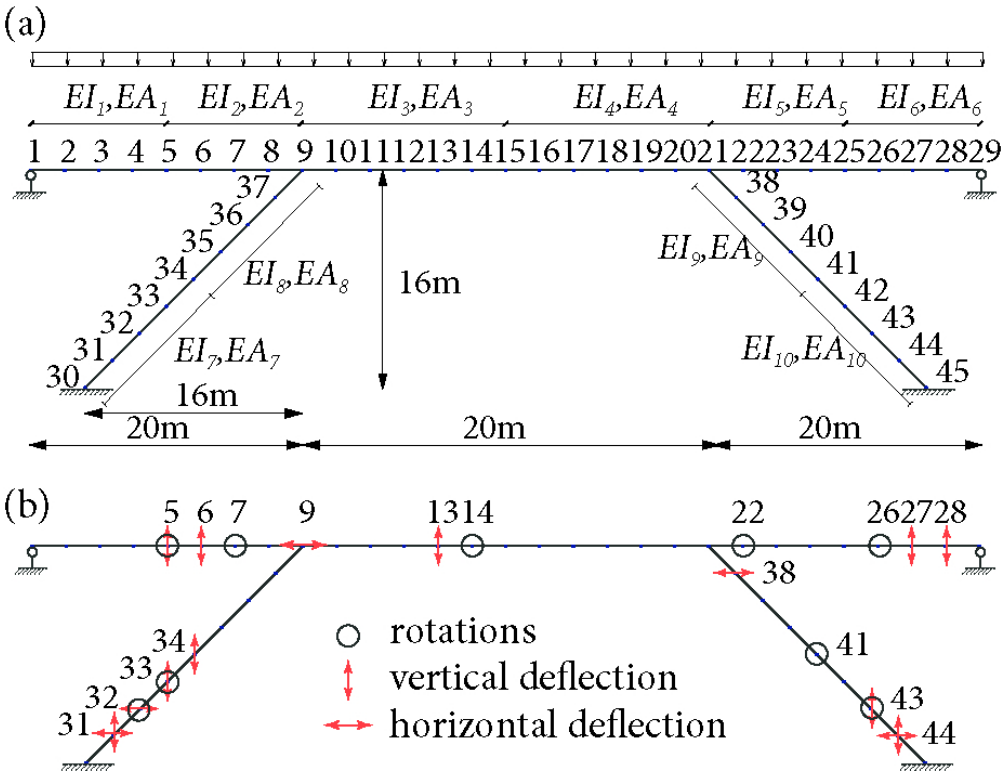

Fig.9 (a) Finite element model and the parameterization of the rigid frame bridge; (b) measurement set of 5 horizontal deflections, 10 vertical deflection and 9 rotations.

78x60mm (300 x 300 DPI)

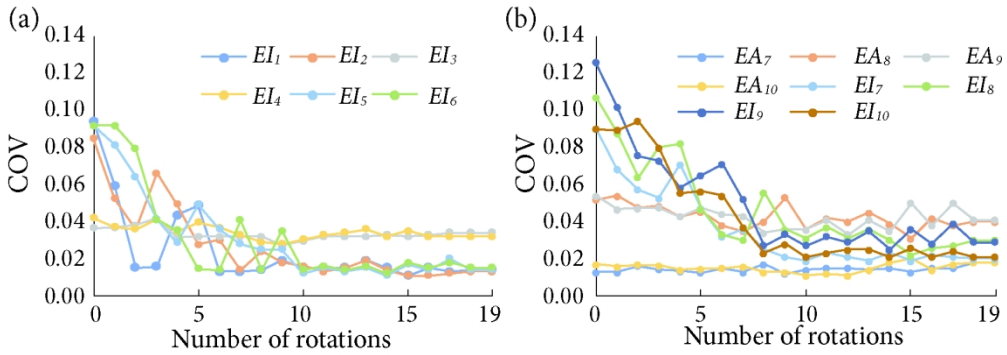

Fig.10 The Coefficients of Variation for the parameters of (a) the decks (EI_1-EI_6); (b) the piers (EA_7-EA_{10},EI_7-EI_{10}).

157x55mm (300 x 300 DPI)